International Journal of Nanomedicine

Dovepress
open access to scientific and medical research

Open Access Full Text Article

ORIGINAL RESEARCH

Surface plasmon-enhanced fluorescence on Au nanohole array for prostate-specific antigen detection

International Journal of Nanomedicine downloaded from https://www.dovepress.com/
For personal use only.

This article was published in the following Dove Press journal:
International Journal of Nanomedicine
27 March 2017
Number of times this article has been viewed

Qingwen Zhang[1,2,*]
Lin Wu[3,*]
Ten It Wong[4]
Jinling Zhang[5]
Xiaohu Liu[5]
Xiaodong Zhou[4]
Ping Bai[3]
Bo Liedberg[5]
Yi Wang[1,2,5]

[1]School of Ophthalmology and Optometry, Eye Hospital, School of Biomedical Engineering, Wenzhou Medical University, [2]Wenzhou Institute of Biomaterials and Engineering, Chinese Academy of Sciences, Wenzhou, People's Republic of China; [3]Electronics and Photonics Department, Institute of High Performance Computing, [4]Institute of Materials Research and Engineering, Agency for Science, Technology and Research (A*STAR), [5]Centre for Biomimetic Sensor Science, School of Materials Science and Engineering, Nanyang Technological University, Singapore

*These authors contributed equally to this work

Correspondence: Yi Wang
Institute of Biomaterials and Engineering, Wenzhou Medical University, No 16 Xinsan Road, Wenzhou 325001, People's Republic of China
Tel +86 577 8801 7535
Email wangyi@wibe.ac.cn

Xiaodong Zhou
Institute of Materials Research and Engineering, Agency for Science, Technology and Research (A*STAR), 3 Research Link, Singapore 117602
Email donna-zhou@imre.a-star.edu.sg

Abstract: Localized surface plasmon (LSP) has been widely applied for the enhancement of fluorescence emission for biosensing owing to its potential for strong field enhancement. However, due to its small penetration depth, LSP offers limited fluorescence enhancement over a whole sensor chip and, therefore, insufficient sensitivity for the detection of biomolecules, especially large molecules. We demonstrate the simultaneous excitation of LSP and propagating surface plasmon (PSP) on an Au nanohole array under Kretschmann configuration for the detection of prostate-specific antigen with a sandwich immunoassay. The proposed method combines the advantages of high field enhancement by LSP and large surface area probed by PSP field. The simulated results indicated that a maximum enhancement of electric field intensity up to 1,600 times can be achieved under the simultaneous excitation of LSP and PSP modes. The sandwich assay of PSA carried out on gold nanohole array substrate showed a limit of detection of 140 fM supporting coexcitation of LSP and PSP modes. The limit of detection was approximately sevenfold lower than that when only LSP was resonantly excited on the same substrate. The results of this study demonstrate high fluorescence enhancement through the coexcitation of LSP and PSP modes and pave a way for its implementation as a highly sensitive bioassay.

Keywords: gold nanohole array, localized surface plasmon, propagating surface plasmon, fluorescence enhancement, prostate-specific antigen

Introduction

Localized surface plasmons (LSPs) are collective electromagnetic oscillations confined to metallic nanostructures, attributed to the interactions between the incident light and metal's surface electrons in its conducting band.[1] This phenomenon has been demonstrated by tremendous applications on chemical and biological sensors.[2–6] Highly enhanced local electromagnetic fields created by the resonantly pumped plasmonic nanostructures result in greatly increased incident light absorption and enhanced emitter excitation, supporting surface-enhanced spectroscopies including surface-enhanced Raman scattering,[7,8] surface-enhanced infrared spectroscopy,[9–11] and surface plasmon-enhanced fluorescence (SPFS).[12–14] Surface plasmons (SPs) with field E_{SP} excited by an incoming light E_0 can enhance fluorophore excitation rate and Raman scattering by factors up to $|E_{sp}/E_0|^2$ and $|E_{sp}/E_0|^4$, respectively.[15–18] Various metal nanostructures have been reported for the enhancement of fluorescence emission, such as nanoholes,[19–21] nanorods,[22,23] core–shell nanoparticles,[24–26] bowtie nanoantennas,[27,28] DNA-assembled nanoparticles,[29] and antennas-in-box.[30] The SPFS based on metallic thin film is usually achieved with Kretschmann configuration by coupling evanescent

© 2017 Zhang et al. This work is published and licensed by Dove Medical Press Limited. The full terms of this license are available at https://www.dovepress.com/terms.php and incorporate the Creative Commons Attribution – Non Commercial (unported, v3.0) License (http://creativecommons.org/licenses/by-nc/3.0/). By accessing the work you hereby accept the Terms. Non-commercial uses of the work are permitted without any further permission from Dove Medical Press Limited, provided the work is properly attributed. For permission for commercial use of this work, please see paragraphs 4.2 and 5 of our Terms (https://www.dovepress.com/terms.php).

waves with SPs, which has been reported for highly sensitive detection of biomolecules including biomarkers,[31,32] toxins, and oligonucleotides,[33] with the limit of detection (LOD) down to attomolar range.[32] The propagating surface plasmon (PSP) typically provides surface field intensity enhancement $|E_{sp}/E_0|^2$ up to 16-fold. The field enhancement by PSP could be further improved up to 60-fold by the excitation of long-range SP on a gold thin film coated on a dielectric layer having its refractive index close to water.[34–37] Compared with the PSP on a metallic thin film, the LSP on metallic nanostructures typically offers higher confinement of the field with a penetration depth L_p from several to tens of nanometers, which is about tenfold lower than the conventional PSP (L_p=180 nm). Such a highly confined LSP field on nanostructures has demonstrated a fluorescence enhancement of about 10- to 200-fold on an averaged area and 1,300-fold for a single dye positioned on the hot spot of a bowtie nanoantenna.[38]

However, the reaction volume on the nanostructures especially in the vicinity confined with high electromagnetic field is typically small, and the average fluorescence enhancement over the whole substrate would be limited. To address this problem and improve field enhancement, combinations of LSP with PSP are considered. Simultaneous excitation of LSP and PSP was demonstrated on a random-distributed gold nanoporous membrane and a silver nanowell substrate.[39,40] However, the field enhancement for fluorescence excitation on this gold nanoporous membrane was not investigated yet. In addition, the coupling of LSP on Au nanoparticles with PSP on Au film was considered as another way to significantly improve the field intensity between the gap of Au nanoparticles and Au film. This method has been reported for surface-enhanced Raman spectroscopy with an enhancement up to 10^7-fold[41] and fluorescence enhancement up to 1,000-fold in such an individual plasmonic gap.[42] However, this method has limited applications, as the gap between the Au nanoparticles and Au film is typically in a range of 5 nm that would not be feasible for the binding of large molecules such as antibodies in terms of biosensing.

In this paper, we simultaneously excited LSP and PSP on Au nanohole arrays under Kretschmann configuration for fluorescence enhancement and accordingly applied the fluorescence for the detection of prostate-specific antigen (PSA) by a sandwich immunoassay. The Au nanohole arrays on a large area were prepared by a high-throughput process based on cost-effective nanoimprinting lithography.[43] Fluorescence enhancement on the Au nanohole arrays by coexcitation of LSP and PSP was directly compared with only LSP mode excited on the same Au nanohole substrate. The coexcited LSP and PSP on the Au nanoholes were expected to provide higher field enhancement and thus there was higher sensitivity compared with the excited LSP alone on the Au nanoholes. Considering the dependence of the fluorescence enhancement on the distance between the dye molecules and the gold surface, we used a sandwich assay to detect PSA on Au nanohole arrays. The sensor response and LOD based on the coexcitation of LSP and PSP were compared with the LSP mode on Au nanohole array.

Materials and methods

Materials

PSA, monoclonal PSA capture antibody (c-Ab), and polyclonal PSA detection antibody (d-Ab) were ordered from SCIPAC Ltd. (Sittingbourne, UK). The triethylene glycol mono-11-mercaptoundecylether (thiol-PEG, #673110), phosphate-buffered saline (PBS) buffer tablets, and Tween-20 buffer were purchased from Sigma-Aldrich Co. (St Louis, MO, USA). The thiol-PEG7 acid (Thiol-COOH, #37156-0795) was purchased from Polypure AS (Oslo, Norway). 1-ethyl-3-(3-dimethylaminopropyl)-carbodiimide and *N*-hydroxysuccinimide were purchased from TCI (Tokyo, Japan). Alexa Fluor 647 protein labeling kit (A-20173) was purchased from Invitrogen (Singapore) for labeling the d-Ab at a dye-to-protein ratio of ~4. Acetate buffer (10 mM, pH 5.0) was prepared by suitable mixing of sodium acetate and acetic acid that were obtained from Sigma-Aldrich Co.

Optical setup

As illustrated in Figure 1A, LSP and PSP on the gold surface were excited by attenuated total reflectance,[37] where the transverse magnetic (p-polarized) beam emitted from a HeNe laser (λ=632.8 nm) was coupled into the attenuated total reflectance through an LASFN9 glass prism (Schott Glass Inc., Mainz, Germany). At the contact area to the prism base, the sensing substrate was applied with matching oil (n=1.700; Cargille Labs, Cedar Grove, NJ, USA) to match its reflective index with the prism. The prism was mounted on a motorized goniometer, and the angular reflectivity spectrum $R(\theta)$ was measured by using a photodiode detector with lock-in amplifier. Aqueous samples (at a refractive index around n_b=1.333) were injected into a flow cell at a rate of 0.4 mL/min using a peristaltic pump, and the total volume of the injected sample was 800 µL. The fluorescent emission from the sensor surface in the flow cell was focused by a lens with a numerical aperture of 0.3 and then passed through two band-pass filters at a central transmission wavelength of 670 nm, followed by intensity detection using a

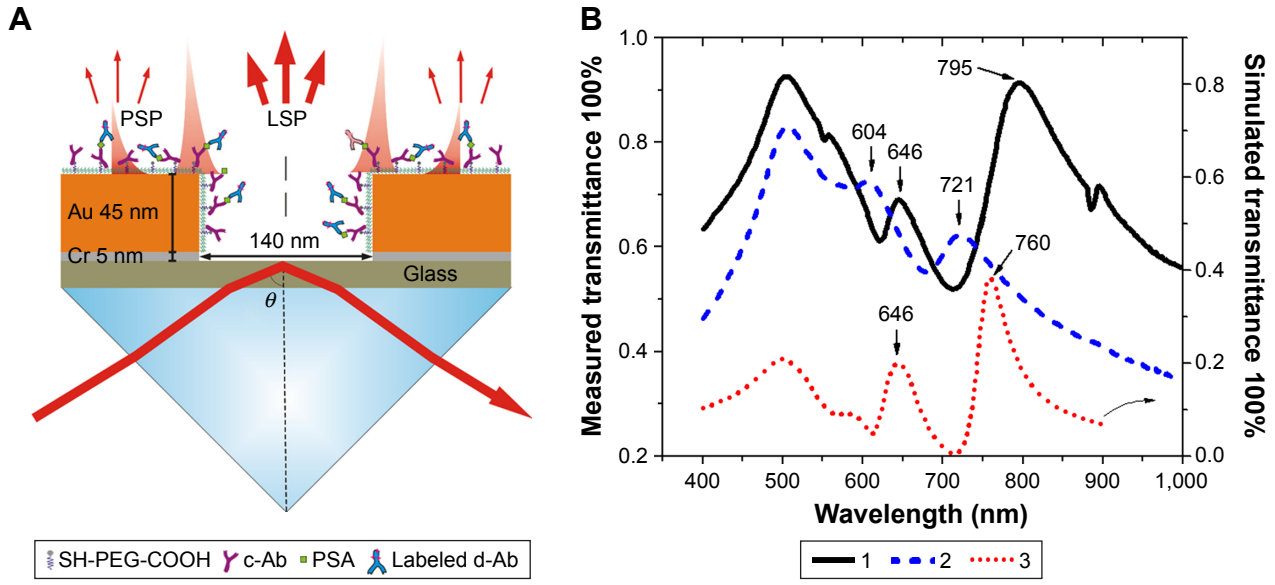

Figure 1 (**A**) Scheme of Au nanohole substrate with prism coupling for surface plasmon-enhanced fluorescence for the sensing of PSA, upon the molecules binding around Au nanohole. (**B**) UV–vis transmission spectra of Au nanohole array measured in (1) water and (2) air, and (3) simulated transmission spectra of Au nanohole array in water.
Abbreviations: PSA, prostate-specific antigen; PSP, propagating surface plasmon; LSP, localized surface plasmon; c-Ab, capture antibody; d-Ab, detection antibody; UV–vis, ultraviolet–visible.

Hamamatsu photomultiplier tube (H6240-01; Hamamatsu Photonics, Hamamatsu, Japan).

Sample fabrication

Au nanohole arrays were mass fabricated by nanoimprinting using a 4″ nickel mold.[43,44] The nickel mold was obtained by electroplating and demolding nickel on a 4″ silicon wafer with resist nanopatterns produced by electron-beam lithography. The Au nanohole arrays were designed to have a pitch *p* of 400 nm, diameter *d* of 140 nm, and thickness *h* of 50 nm (5 nm chromium and 45 nm of Au). Briefly, the Au nanohole array was fabricated by nanoimprinting the nickel mold on a ultraviolet (UV)-curable photoresist layer (mr-UVCur21-300 nm; micro resist technology GmbH, Berlin, Germany) coated on a 4″ glass wafer. The nanoimprinted patterns went through reactive ion etching to expose the glass surface with an indented photoresist. Chromium film (5 nm) and gold film (45 nm) were subsequently deposited on the processed glass wafer, and the photoresist was removed by plasma etching to acquire the Au-hole array. The fabricated nanoholes were rinsed with acetone and isopropyl alcohol before use.

Surface modification

PSA was detected by immersing Au nanohole substrates in ethanol solution with 0.1 mM thiol-COOH and 0.9 mM thiol-PEG for overnight. Afterward, the substrates were rinsed with ethanol and blown dried with N_2, and mounted in a flow cell (at a volume of 100 µL) which allows the circulation of buffer with a peristaltic pump. Freshly prepared 1-ethyl-3-(3-dimethylaminopropyl)-carbodiimide (37.5 mg/mL) and *N*-hydroxysuccinimide (11.5 mg/mL) in deionized water were flushed into the flow cell to activate the carbon acid groups on the sensing substrate. c-Ab was anchored on the carbon acid group by incubating the substrate in 50 µg/mL c-Ab acetate buffer (pH 5.0) for 90 minutes.

Sandwich immunoassay of PSA

PBS-Tween 20 (PBST) buffer with various PSA concentrations was used as samples for sandwich assay of PSA. PSA immunoassay was performed by first incubating PSA samples with c-Ab-modified substrates for 30 minutes in flow cell, then rinsing with PBST for 2–3 minutes, and injecting d-Ab (10 nM in PBST) for 20 minutes. The fluorescence intensity was read after a 5-minute rinse with PBST buffer. The substrate was regenerated by rinsing with 0.1 M HCl for 30 seconds before the injection of the next PSA sample.

Simulation method

COMSOL Multiphysics, which solves Maxwell equations with finite element method (FEM), was applied to simulate the plasmons. The dielectric function of Au for different wavelengths was obtained from the handbook by Palik and Ghosh.[45] The refractive indices of air, water-based buffer, and glass substrate were set as 1, 1.33, and 1.52, respectively. Only a unit cell including one nanohole was simulated by setting Floquet periodic boundary condition at the sides

of the unit cell. Obliquely incident and linearly polarized white light (400–900 nm) struck on the Au nanohole array, and the light was absorbed, reflected, or transmitted. The absorbed power was calculated by integrating the resistive heating within the volume of the Au nanostructures, and the reflected or transmitted power was computed by integrating the power flow on a far-field surface.[46] The lump sum power of the simulated absorption, reflection, and transmission was compared to the power of the incident light to evaluate the simulation accuracy. Furthermore, the near-field power distributions on the nanoholes at the resonant wavelengths were directly obtained by the simulations.

Results and discussion

Characterization of nanostructures

The gold nanohole array substrates were fabricated based on nanoimprinted lithography, which is compatible with roll-to-roll printing and can be easily applied for high-throughput manufacture. The AFM measurement indicated that the fabricated nanoholes have a diameter *d* of 140 nm, a pitch *p* of 400 nm, and a thickness *h* of 50 nm, as reported in our previous work.[43,44,47] Figure 1A shows the schematic structure of gold nanohole and the plasmon-coupling method based on Kretschmann configuration. These parameters were optimized to have the plasmon mode overlapping with the excitation wavelength of Alexa 647 (λ_{ex}=647 nm).[46] The ultraviolet–visible transmission spectrum of Au nanohole array in air showed two plasmon resonant peaks: λ_1=604 nm for α plasmon mode on the top rims of the Au nanoholes and λ_2=721 nm for β plasmon mode on the bottom rims of the Au nanoholes (Figure 1B).[44] These two peaks shifted to higher wavelength of λ_1=646 nm and λ_2=795 nm as measured in water, due to the higher refractive index of water (n_{water}=1.333) than air (n_{air}=1). The peak at λ=500 nm indicated that the interband transition intrinsically exists in gold.[48,49] An FEM simulation, carried out on Au nanohole with a hole diameter *d* of 140 nm, a pitch *p* of 400 nm, and a thickness *h* of 50 nm, indicated the α and β plasmon peaks at λ_1=646 nm and λ_2=760 nm, which were comparable to the experimental results as measured in water (Figure 1B).

Au nanohole arrays were used for the fluorescence enhancement based on LSP excitation with a typical electric field enhancement of $|E_{sp}/E_0|^2 > 50$ at a normal incident angle, which is able to improve the sensitivity by a factor of >10.[21,44] However, the strong electric field was only located around the top and bottom rims of the nanohole with a maximum field enhancement of $|E_{sp}/E_0|^2$ =100, at a wavelength of λ=632.8 nm for an incident angle of 62.3° (Figure 2A and B),

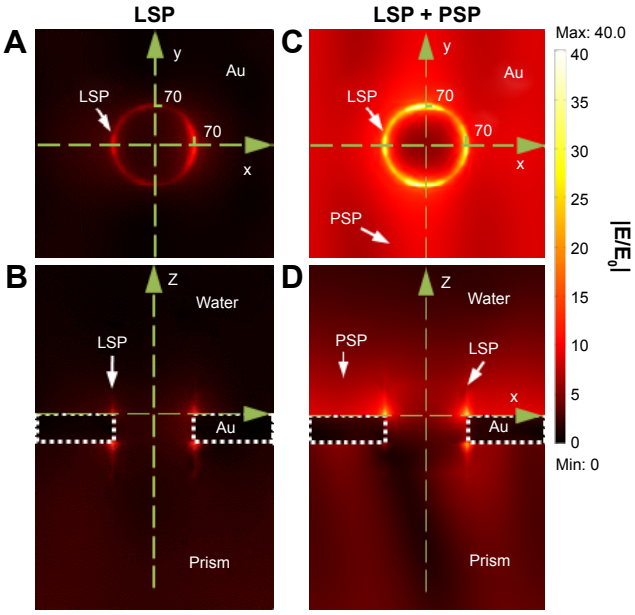

Figure 2 (**A** and **C**) The top views and (**B** and **D**) cross-sectional views of simulated distribution of electric field amplitude $|E/E_0|$ for Au nanohole with (**A** and **B**) LSP mode and (**C** and **D**) coexcited LSP and PSP modes at λ=632.8 nm with incident angles of 62.3° and 73°, respectively.
Abbreviations: LSP, localized surface plasmon; Max, maximum; min, minimum; PSP, propagating surface plasmon.

where only LSP mode was excited. In addition, due to the small field penetration depth, the rest of the Au surface had very limited field intensity and, therefore, low average field enhancement (Figure 2A and B). Compared with LSP, PSP has longer penetration depth and larger field coverage, but relatively lower field enhancement. To take advantage of both the PSP and LSP, we employed Au nanohole array for the simultaneous excitation of LSP and PSP for fluorescence enhancement with Kretschmann configuration and an incident p-polarized laser light of λ=632.8 nm (Figure 1A). The FEM simulation indicated that the field was strongly localized around the top and bottom rims of Au nanohole with a maximum field intensity enhancement up to a factor of $|E_{sp}/E_0|^2$ =1,600 (Figure 2C and D) at an incident angle of 73°, where the LSP and PSP were coexcited. The maximum field enhancement was ~16-fold higher than the LSP mode ($|E_{sp}/E_0|^2$ =100) excited on Au nanohole array (Figure 2A and B; Table 1). In addition, the field intensity other than the

Table 1 LOD for the detection of PSA on Au nanohole array substrates with LSP mode and coexcited LSP and PSP modes

	LSP	LSP + PSP
Maximum enhancement factor, $\|E/E_0\|^2$	100	1,600
PSA (LOD)	0.94 pM	140 fM

Abbreviations: LOD, limit of detection; PSA, prostate-specific antigen; LSP, localized surface plasmon; PSP, propagating surface plasmon.

rim of nanohole also showed much higher field enhancement as compared with the LSP mode (Figure 2A and C).

In order to explore the details of the field enhancement upon coupling of LSP and PSP modes, cross-sections of the electric field amplitude $|E/E_0|$ in the vicinity of nanoholes are plotted in Figure 3. These plots show that the field amplitude decays exponentially away from the surface for LSP mode and coexcited LSP and PSP modes (Figure 3A and B). The field amplitude $|E/E_0|$ of LSP mode on Au nanohole surface decays from 10-fold (at x=70 nm, y=0) to 1-fold (at z=50 nm) as shown in Figure 3B. The electric field amplitude $|E/E_0|$ for coexcited LSP and PSP modes shows higher field amplitude and longer penetration depth with $|E/E_0| \geq 5$ at $z \leq 100$ nm. Similarly, the lateral field distribution along the y-axis indicates that the overall field amplitude $|E/E_0|$ due to coexcited LSP and PSP at the Au nanohole substrate is about 4- to 15-fold higher than the LSP mode (Figure 3C and D). In addition, the field intensity for LSP mode is only confined in the vicinity of Au nanohole within a ~100 nm circle concentric with the nanohole, while for the coexcited LSP and PSP modes, the field amplitude $|E/E_0|$ is nearly constant at 7- to 10-fold within a 200 nm radius circle concentric with the nanohole. This is due to the excitation of PSP mode that has longer propagating length and larger field intensity.

Sandwich immunoassay of PSA

To prove the concept that the fluorescence coenhanced by LSP and PSP could improve the sensitivity for the detection of molecules, we compared the Au nanohole at 73° (coexcitation of LSP and PSP modes) and 62.3° (LSP mode) with a sandwich

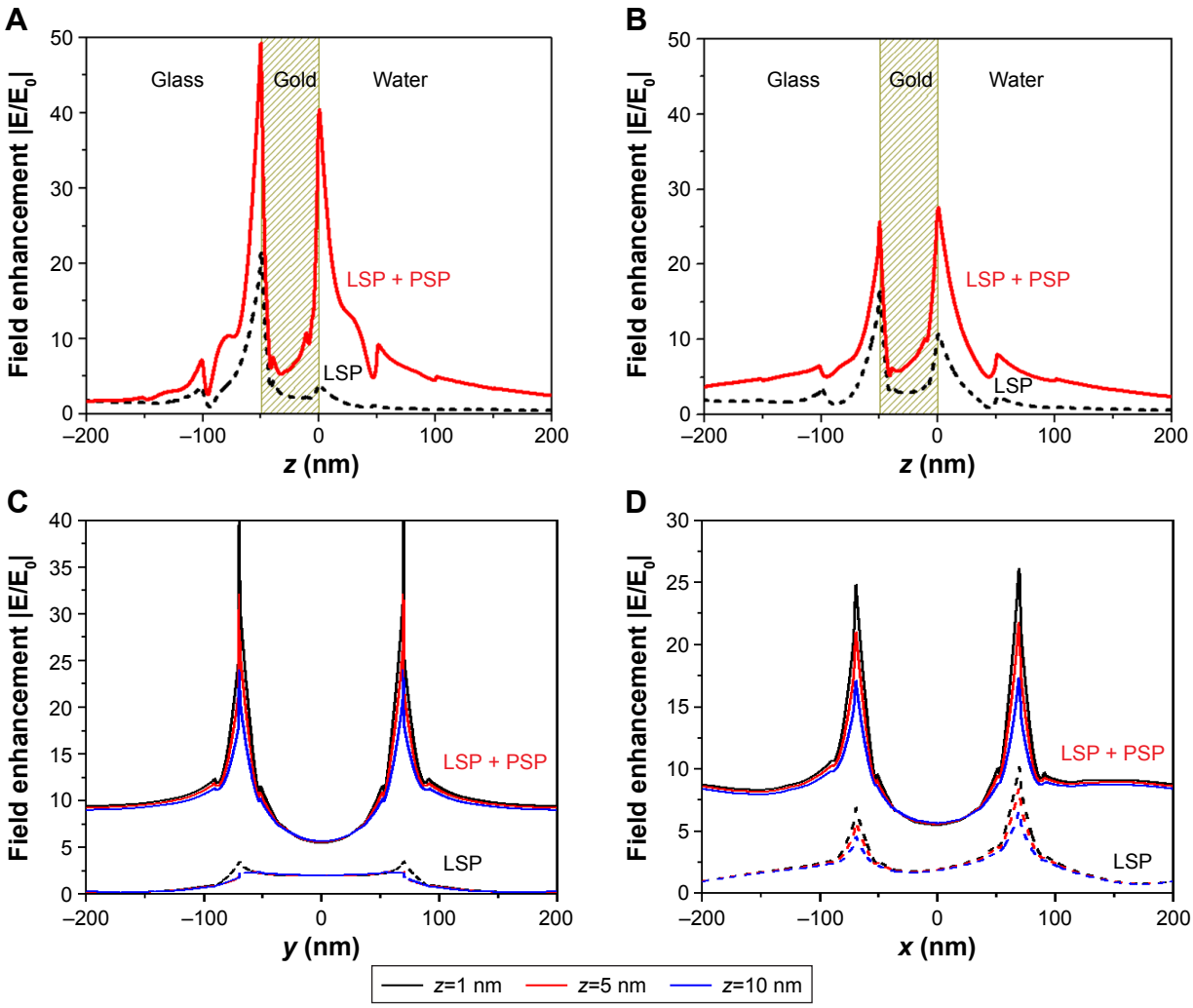

Figure 3 The simulated electric field amplitude $|E/E_0|$ as a function of distance z from the surface, for the resonant excitation of LSP (dashed lines) and coexcited LSP and PSP (solid lines) on Au nanohole array substrate at λ=632.8 nm. The field distributions are plotted for (**A**) x=0, y=70 nm and (**B**) x=70 nm, y=0. (**C** and **D**) The electric field amplitude $|E/E_0|$ as a function of lateral distance for different heights above the surface z=1, 5, and 10 nm for the resonant excitation of LSP (dashed lines) and coexcited LSP and PSP (solid lines). The field distributions are plotted for (**C**) x=0, z=1, 5, and 10 nm and (**D**) y=0, z=1, 5, and 10 nm. The cross points of x, y, and z axes are x=y=z=0.
Abbreviations: LSP, localized surface plasmon; PSP, propagating surface plasmon.

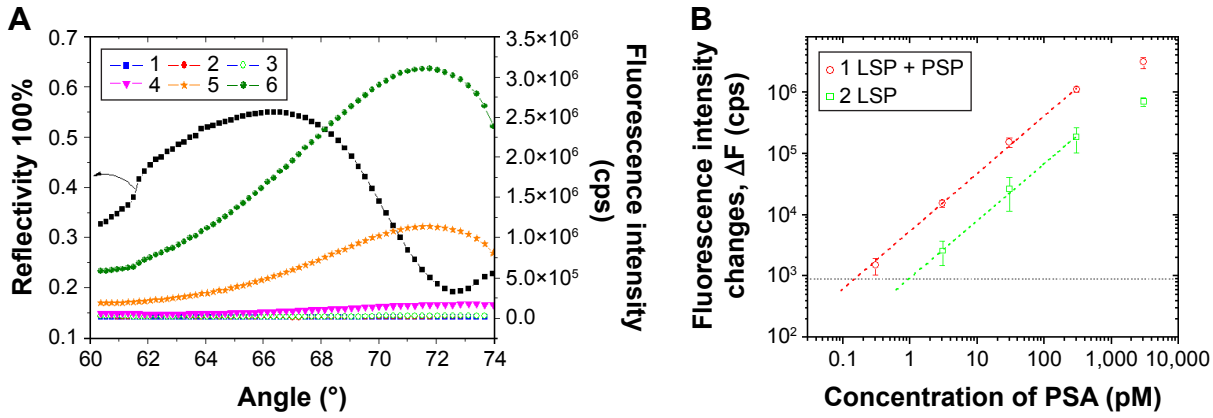

Figure 4 (**A**) The angular SPR reflectivity (black square) and fluorescence spectra of Au nanohole array for the sandwich assay of PSA at concentrations of (1) 0, (2) 300 fM, (3) 3 pM, (4) 30 pM, (5) 300 pM, and (6) 3 nM. (**B**) Calibration curves for PSA detection based on Au nanohole with (1) coexcited LSP and PSP modes and (2) LSP mode. Error bars were obtained from the measurements on three different chips.

Abbreviations: SPR, surface plasmon resonance; PSA, prostate-specific antigen; LSP, localized surface plasmon; PSP, propagating surface plasmon.

assay for PSA detection. The angular reflectivity spectrum of Au nanohole arrays showed a minimum reflectance at ~73°, which is due to the excitation of PSP mode (Figure 4A). While at the incident angle of 62.3°, only LSP mode was excited and PSP mode was negligible. After the immobilization of c-Ab, affinity immunoassay of PSA was investigated upon injecting a PSA solution at concentrations of 0–3 nM into the flow cell, followed by 10 nM d-Ab injection. Meanwhile, the fluorescence intensity was monitored at incident angles of 62.3° and 73°. The coexcited PSP and LSP localized on the Au nanohole array provided fluorescence intensity changes up to 3.1×10^6 cps (Figure 4A), which is ~4.4 times higher than that excited by LSP only on the Au nanohole (7×10^5 cps).

The calibration curve in Figure 4B shows linear response with PSA concentration from 0.3 pM to 3 nM, and the response tends to saturate at a concentration of PSA >3 nM. The calibration curve also indicated an LOD for the detection of PSA down to 140 fM on Au nanohole substrate with coexcited LSP and PSP, which is about seven times higher than the LSP mode on Au nanohole (LOD =0.94 pM) at 62.3° (Table 1). The LOD was determined by the concentration of PSA whose signal equals to three times the standard deviation of the blank samples' response (Figure 4B). The sensitivity of this method is comparable with that of the long-range SP-enhanced fluorescence based on three-dimensional hydrogel-binding matrix (34 fM).[37] However, it is two orders higher sensitivity than SP resonance direct detection (LOD of 30 pM).[50] Overall, the coexcitation of LSP and PSP could significantly improve the field intensity around the nanostructures and thus improve fluorescence enhancement as compared with the case where only LSP was excited. In addition, the coexcitation of LSP and PSP has shown enhancement in a label-free sensor scheme for the detection of IgG on a microhole array substrate by monitoring the resonant wavelength shift.[51]

Conclusion

We have demonstrated the coexcitation of LSP and PSP for fluorescence enhancement on Au nanohole array substrates with Kretschmann configuration. This method allowed concentrating the electromagnetic field around Au nanohole, which theoretically provided up to 1,600-fold higher field intensity enhancement. In addition, the experimental investigation on the fluorescence enhancement indicated that compared with LSP mode alone excited on Au nanohole, the sensitivity of the sandwich assay of PSA on Au nanohole array substrates with the coexcitation of LSP and PSP was improved by sevenfold and the LOD decreased down to 140 fM for the detection of PSA. The future work includes the improvement of nanostructure for high enhancement of fluorescence intensity and possibility for highly directional fluorescence emission.[52] We believe that the method of simultaneously exciting LSP and PSP modes for fluorescence enhancement would pave the way to significantly improve the sensitivity of molecule detection and offers as a potential candidate for the early cancer diagnosis and food safety monitoring.

Acknowledgments

The authors express their sincere gratitude to the National Natural Science Foundation of China (201605116), Public Projects of Zhejiang Province (2017C33193), Public Projects of Wenzhou (Y20160065, Y20160067), and the Government of Wenzhou, People's Republic of China, for the financial support, the startup fund WIBEZD2014004-02,

and Science & Engineering Research Council of Agency for Science, Technology and Research (A*STAR), Singapore, for TSRP projects 1021520014 and 1021520015.

Disclosure

The authors report no conflicts of interest in this work.

References

1. Willets KA, Van Duyne RP. Localized surface plasmon resonance spectroscopy and sensing. *Annu Rev Phys Chem*. 2007;58(1):267–297.
2. Mayer KM, Hafner JH. Localized surface plasmon resonance sensors. *Chem Rev*. 2011;111(6):3828–3857.
3. Haes AJ, Van Duyne RP. A nanoscale optical biosensor: sensitivity and selectivity of an approach based on the localized surface plasmon resonance spectroscopy of triangular silver nanoparticles. *J Am Chem Soc*. 2002;124(35):10596–10604.
4. Bauch M, Toma K, Toma M, Zhang Q, Dostalek J. Plasmon-enhanced fluorescence biosensors: a review. *Plasmonics*. 2014;9(4):781–799.
5. Liu F, Zhang X. Fano coupling between Rayleigh anomaly and localized surface plasmon resonance for sensor applications. *Biosens Bioelectron*. 2015;68:719–725.
6. Zhao Q, Duan R, Yuan J, Quan Y, Yang H, Xi M. A reusable localized surface plasmon resonance biosensor for quantitative detection of serum squamous cell carcinoma antigen in cervical cancer patients based on silver nanoparticles array. *Int J Nanomedicine*. 2014;9:1097–1104.
7. Toderas F, Baia M, Baia L, Astilean S. Controlling gold nanoparticle assemblies for efficient surface-enhanced Raman scattering and localized surface plasmon resonance sensors. *Nanotechnology*. 2007;18(25):255702.
8. Hossain MK, Kitahama Y, Huang GG, Han X, Ozaki Y. Surface-enhanced Raman scattering: realization of localized surface plasmon resonance using unique substrates and methods. *Anal Bioanal Chem*. 2009;394(7):1747–1760.
9. Rowe DJ, Jeong JS, Mkhoyan KA, Kortshagen UR. Phosphorus-doped silicon nanocrystals exhibiting mid-infrared localized surface plasmon resonance. *Nano Lett*. 2013;13(3):1317–1322.
10. Liu X, Wang X, Zhou B, Law W-C, Cartwright AN, Swihart MT. Size-controlled synthesis of $Cu_{2-x}E$ (E = S, Se) nanocrystals with strong tunable near-infrared localized surface plasmon resonance and high conductivity in thin films. *Adv Funct Mater*. 2013;23(10):1256–1264.
11. Chou L-W, Shin N, Sivaram SV, Filler MA. Tunable mid-infrared localized surface plasmon resonances in silicon nanowires. *J Am Chem Soc*. 2012;134(39):16155–16158.
12. Zoriniants G, Barnes WL. Fluorescence enhancement through modified dye molecule absorption associated with the localized surface plasmon resonances of metallic dimers. *New J Phys*. 2008;10(10):105002.
13. Wang HS, Xiao FN, Li ZQ, et al. Sensitive determination of reactive oxygen species in cigarette smoke using microchip electrophoresis-localized surface plasmon resonance enhanced fluorescence detection. *Lab Chip*. 2014;14(6):1123–1128.
14. Bu Y, Lee S-W. The characteristic $Ag_{core}Au_{shell}$ nanoparticles as SERS substrates in detecting dopamine molecules at various pH ranges. *Int J Nanomedicine*. 2015;10:47–54.
15. Fort E, Grésillon S. Surface enhanced fluorescence. *J Phys D Appl Phys*. 2008;41(1):013001.
16. Johansson P, Xu HX, Käll M. Surface-enhanced Raman scattering and fluorescence near metal nanoparticles. *Phys Rev B*. 2005;72(3):035427.
17. Xu HX, Wang XH, Persson MP, Xu HQ, Käll M, Johansson P. Unified treatment of fluorescence and Raman scattering processes near metal surfaces. *Phys Rev Lett*. 2004;93(24):243002.
18. Le Ru EC, Etchegoin PG. Rigorous justification of the $[E]^4$ enhancement factor in surface enhanced Raman spectroscopy. *Chem Phys Lett*. 2006;423(1–3):63–66.
19. Chang SH, Gray S, Schatz G. Surface plasmon generation and light transmission by isolated nanoholes and arrays of nanoholes in thin metal films. *Opt Express*. 2005;13(8):3150–3165.
20. Brolo AG, Gordon R, Leathem B, Kavanagh KL. Surface plasmon sensor based on the enhanced light transmission through arrays of nanoholes in gold films. *Langmuir*. 2004;20(12):4813–4815.
21. Brolo AG, Kwok SC, Moffitt MG, Gordon R, Riordon J, Kavanagh KL. Enhanced fluorescence from arrays of nanoholes in a gold film. *J Am Chem Soc*. 2005;127(42):14936–14941.
22. Knappenberger KL, Wong DB, Xu W, et al. Excitation-wavelength dependence of fluorescence intermittency in CdSe nanorods. *ACS Nano*. 2008;2(10):2143–2153.
23. Ming T, Zhao L, Yang Z, et al. Strong polarization dependence of plasmon-enhanced fluorescence on single gold nanorods. *Nano Lett*. 2009;9(11):3896–3903.
24. Bardhan R, Grady NK, Cole JR, Joshi A, Halas NJ. Fluorescence enhancement by Au nanostructures: nanoshells and nanorods. *ACS Nano*. 2009;3(3):744–752.
25. Pang Y, Rong Z, Wang J, Xiao R, Wang S. A fluorescent aptasensor for H5N1 influenza virus detection based-on the core-shell nanoparticles metal-enhanced fluorescence (MEF). *Biosens Bioelectron*. 2015;66:527–532.
26. Ma H, Li B, Zhang L, Han D, Zhu G. Targeted synthesis of core–shell porous aromatic frameworks for selective detection of nitro aromatic explosives via fluorescence two-dimensional response. *J Mater Chem A*. 2015;3(38):19346–19352.
27. Kinkhabwala AA, Yu Z, Fan S, Moerner WE. Fluorescence correlation spectroscopy at high concentrations using gold bowtie nanoantennas. *Chem Phys*. 2012;406:3–8.
28. Nien L-W, Lin S-C, Chao B-K, Chen M-J, Li J-H, Hsueh C-H. Giant electric field enhancement and localized surface plasmon resonance by optimizing contour bowtie nanoantennas. *J Phys Chem C*. 2013;117(47):25004–25011.
29. Acuna GP, Möller FM, Holzmeister P, Beater S, Lalkens B, Tinnefeld P. Fluorescence enhancement at docking sites of DNA-directed self-assembled nanoantennas. *Science*. 2012;338(6106):506–510.
30. Punj D, Mivelle M, Moparthi SB, et al. A plasmonic 'antenna-in-box' platform for enhanced single-molecule analysis at micromolar concentrations. *Nat Nanotechnol*. 2013;8(7):512–516.
31. Yu F, Yao DF, Knoll W. Surface plasmon field-enhanced fluorescence spectroscopy studies of the interaction between an antibody and its surface-coupled antigen. *Anal Chem*. 2003;75(11):2610–2617.
32. Yu F, Persson B, Löfås S, Knoll W. Surface plasmon fluorescence immunoassay of free prostate-specific antigen in human plasma at the femtomolar level. *Anal Chem*. 2004;76(22):6765–6770.
33. Yao DF, Yu F, Kim J, et al. Surface plasmon field-enhanced fluorescence spectroscopy in PCR product analysis by peptide nucleic acid probes. *Nucleic Acids Res*. 2004;32(22):e177.
34. Kasry A, Knoll W. Long range surface plasmon fluorescence spectroscopy. *Appl Phys Lett*. 2006;89(10):101106.
35. Dostalek J, Kasry A, Knoll W. Long range surface plasmons for observation of biomolecular binding events at metallic surfaces. *Plasmonics*. 2007;2(3):97–106.
36. Wang Y, Dostalek J, Knoll W. Long range surface plasmon-enhanced fluorescence spectroscopy for the detection of aflatoxin M1 in milk. *Biosens Bioelectron*. 2009;24(7):2264–2267.
37. Wang Y, Brunsen A, Jonas U, Dostalek J, Knoll W. Prostate specific antigen biosensor based on long range surface plasmon-enhanced fluorescence spectroscopy and dextran hydrogel binding matrix. *Anal Chem*. 2009;81(23):9625–9632.
38. Rivoire K, Kinkhabwala A, Hatami F, et al. Lithographic positioning of fluorescent molecules on high-*Q* photonic crystal cavities. *Appl Phys Lett*. 2009;95(12):123113.

39. Yu F, Ahl S, Caminade AM, Majoral JP, Knoll W, Erlebacher J. Simultaneous excitation of propagating and localized surface plasmon resonance in nanoporous gold membranes. *Anal Chem*. 2006;78(20):7346–7350.
40. Wang XN, Wang YY, Cong M, et al. Propagating and localized surface plasmons in hierarchical metallic structures for surface-enhanced raman scattering. *Small*. 2013;9(11):1895–1899.
41. Liu Y, Xu S, Li H, Jian X, Xu W. Localized and propagating surface plasmon co-enhanced Raman spectroscopy based on evanescent field excitation. *Chem Commun (Camb)*. 2011;47(13):3784–3786.
42. Schmelzeisen M, Zhao Y, Klapper M, Mullen K, Kreiter M. Fluorescence enhancement from individual plasmonic gap resonances. *ACS Nano*. 2010;4(6):3309–3317.
43. Wong TI, Han S, Wu L, et al. High throughput and high yield nanofabrication of precisely designed gold nanohole arrays for fluorescence enhanced detection of biomarkers. *Lab Chip*. 2013;13(12):2405–2413.
44. Wang Y, Wu L, Zhou X, et al. Incident-angle dependence of fluorescence enhancement and biomarker immunoassay on gold nanohole array. *Sens Actuators B Chem*. 2013;186:205–211.
45. Palik ED, Ghosh G. *Handbook of Optical Constants of Solids*. San Diego, CA: Academic Press; 1998.
46. Wu L, Bai P, Li EP. Designing surface plasmon resonance of subwavelength hole arrays by studying absorption. *J Opt Soc Am B*. 2012;29(4):521–528.
47. Zhang J, Wang Y, Wong TI, Liu X, Zhou X, Liedberg B. Electrofocusing-enhanced localized surface plasmon resonance biosensors. *Nanoscale*. 2015;7(41):17244–17248.
48. Shuford KL, Ratner MA, Gray SK, Schatz GC. Finite-difference time-domain studies of light transmission through nanohole structures. *Appl Phys B*. 2006;84(1–2):11–18.
49. Gao HW, Henzie J, Odom TW. Direct evidence for surface plasmon-mediated enhanced light transmission through metallic nanohole arrays. *Nano Lett*. 2006;6(9):2104–2108.
50. Huang L, Reekmans G, Saerens D, et al. Prostate-specific antigen immunosensing based on mixed self-assembled monolayers, camel antibodies and colloidal gold enhanced sandwich assays. *Biosens Bioelectron*. 2005;21(3):483–490.
51. Live LS, Dhawan A, Gibson KF, et al. Angle-dependent resonance of localized and propagating surface plasmons in microhole arrays for enhanced biosensing. *Anal Bioanal Chem*. 2012;404(10):2859–2868.
52. Wang Y, Wu L, Wong TI, et al. Directional fluorescence emission co-enhanced by localized and propagating surface plasmons for biosensing. *Nanoscale*. 2016;8(15):8008–8016.

International Journal of Nanomedicine

Dovepress

Publish your work in this journal

The International Journal of Nanomedicine is an international, peer-reviewed journal focusing on the application of nanotechnology in diagnostics, therapeutics, and drug delivery systems throughout the biomedical field. This journal is indexed on PubMed Central, MedLine, CAS, SciSearch®, Current Contents®/Clinical Medicine, Journal Citation Reports/Science Edition, EMBase, Scopus and the Elsevier Bibliographic databases. The manuscript management system is completely online and includes a very quick and fair peer-review system, which is all easy to use. Visit http://www.dovepress.com/testimonials.php to read real quotes from published authors.

Submit your manuscript here: http://www.dovepress.com/international-journal-of-nanomedicine-journal